We are IntechOpen, the world's leading publisher of Open Access books Built by scientists, for scientists

4,800
Open access books available

122,000
International authors and editors

135M
Downloads

Our authors are among the

154
Countries delivered to

TOP 1%
most cited scientists

12.2%
Contributors from top 500 universities

CLARIVATE ANALYTICS BOOK CITATION INDEX INDEXED

WEB OF SCIENCE™

Selection of our books indexed in the Book Citation Index in Web of Science™ Core Collection (BKCI)

Interested in publishing with us?
Contact book.department@intechopen.com

Numbers displayed above are based on latest data collected.
For more information visit www.intechopen.com

4

Simulation of 3-D Coastal Spit Geomorphology Using Differential Synthetic Aperture Interferometry (DInSAR)

Maged Marghany
Institute for Science and Technology Geospatial (INSTEG)
Universiti Teknologi Malaysia, Skudai, Johor Bahru,
Malaysia

1. Introduction

Interferometric synthetic aperture radar (InSAR or IfSAR), is a geodetic technique uses two or more single look complex synthetic aperture radar (SAR) images to produce maps of surface deformation or digital elevation (Massonnet, and Feigl 1998; Burgmann et al., 2000; Hanssen 2001). It has applications as well, for monitoring of geophysical natural hazards, for instance earthquakes, volcanoes and landslides, also in engineering, in particular recording of subsidence and structural stability. Over time-spans of days to years, InSAR can detect the centimetre-scale of deformation changes (Zebker et al.,1997). Further, the precision DEMs with of a couple of ten meters can produce from InSAR technique compared to conventional remote sensing methods. Nevertheless, the availability of the precision DEMs may a cause of two-pass InSAR; regularly 90 m SRTM data may be accessible for numerous territories (Askne et al.,2003). InSAR, consequently, provides DEMs with 1-10 cm accuracy, which can be improved to millimetre level by DInSAR. Even so, alternative datasets must acquire at high latitudes or in areas of rundown coverage (Nizalapur et al., 2011). However, the baseline decorrelation and temporal decorrelation make InSAR measurements unfeasible (Lee 2001; Luo et al., 2006; Yang et al., 2007; Rao and Jassar 2010). In this regard, Gens (2000) reported the length of the baseline designates the sensitivity to height changes and sum of baseline decorrelation. Further, Gens (2000) stated the time difference for two data acquisitions is a second source of decorrelation. Indeed, the time differences while comparing data sets with a similar baseline length acquired one and 35 days a part suggests only the temporal component of the decorrelation. Therefore, the loss of coherence in the same repeat cycle in data acquisition are most likely because of baseline decorrelation. According to Roa et al. (2006), uncertainties could arise in DEM because of limitation InSAR repeat passes. In addition, the interaction of the radar signal with troposphere can also induce decorrelation. This is explained in several studies of Hanssen (2001); Marghany and Hashim (2009); and Rao and Jassar (2010).

Generally, the propagation of the waves through the atmosphere can be a source of error exist in most interferogram productions. When the SAR signal propagated through a

vacuum it should theoretically be subjected to some decent accuracy of timing and cause phase delay (Hanssen 2001). A constant phase difference between the two images caused by the horizontally homogeneous atmosphere was over the length scale of an interferogram and vertically over that of the topography. The atmosphere, however, is laterally heterogeneous on length scales both larger and smaller than typical deformation signals (Lee 2001). In other cases the atmospheric phase delay, however, is caused by vertical inhomogeneity at low altitudes and this may result in fringes appearing to correspond with the topography. Under this circumstance, this spurious signal can appear entirely isolated from the surface features of the image, since the phase difference is measured other points in the interferogram, would not contribute to the signal (Hanssen 2001). This can reduce seriously the low signal-to-noise ratio (SNR) which restricted to perform phase unwrapping. Accordingly, the phases of weak signals are not reliable. According to Yang et al., (2007), the correlation map can be used to measure the intensity of the noise in some sense. It may be overrated because of an inadequate number of samples allied with a small window (Lee 2001). Weights are initiated to the correlation coefficients according to the amplitudes of the complex signals to estimate accurate reliability (Yang et al., 2007).

1.1 Hypothesis and objective of study

Concerning with above prospective, we address the question of decorrelation uncertainties impact on modelling Digital Elevation Model (DEM) for 3-D coastal spit visualization from DInSAR technique. This is demonstrated with RADARSAT-1 fine mode data (F1) using fuzzy B-spline algorithm. Taking advantage of the fact that fuzzy B-spline can use for solving uncertainty problem because of decorrelation and the low signal-to-noise ratio (SNR) in data sets. This work hypothesises that integration of fuzzy B-spline algorithm with phase unwrapping can produce accurately digital elevation of object deformation (Marghany et al., 2010a and Marghany 2012). The aim of this paper is to explore the precision of the digital elevation models (DEM) derived from RADARSAT-1 fine mode data (F1) and, thus, the potential of the sensor for mapping coastal geomorphologic feature changes. Depending on the results, a wider application of F1 mode data for the study of Kuala Terengganu mouth river landscapes is envisaged.

2. Study area

The study area is selected along the mouth river of Kuala Terengganu, Malaysia. According to Marghany et al., (2010a) the coastline appears to be linear and oriented at about 45° along the east coast of Malaysia (Marghany et al. 2010b). In addition, spit was located across the largest hydrological communications between the estuary and the South China Sea the i.e. mouth river of Kuala Terengganu (Fig. 1) which lies on the equatorial region, and is affected by monsoon winds (Marghany and Mazlan 2010a,b). Indeed, during the northeast monsoon period, the strong storm and wave height of 4 m can cause erosion (Marghany et al. 2010b). The 20 km stretches of coastal along the Kuala Terengganu shoreline composed of sandy beach, the somewhat most frequently eroded region. The significant source of sediment is from the Terengganu River which loses to the continental shelf due to the complex movements of waves approached from the north direction (Marghany et al. 2010b).

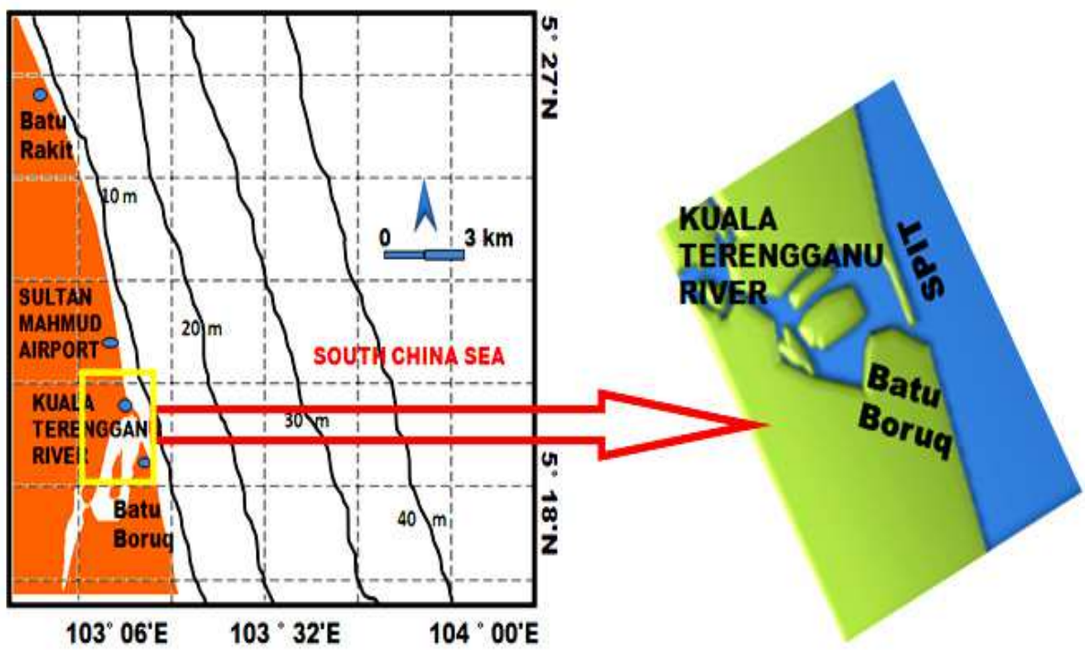

Fig. 1. Location of spit along Kuala Terengganu river mouth.

3. Data sets

3.1 Satellite data

In the present study, RADARSAT-1 SAR data sets of 23 November 1999 (SLC-1), 23 December 2003 (SLC-2) and March 26, 2005, (SLC-3) of Fine mode data (F1) are implemented. These data are C-band and had the lower signal-to-noise ratio owing to their HH polarization with wavelength of 5.6 cm and frequency of 5.3 GHz. The Fine beam mode is intended for applications which require the best spatial resolution available from the RADARSAT-1 SAR system. The azimuth resolution is 8.4 m, and range resolution ranges between 9.1 m to 7.8 m. Originally, five Fine beam positions, F1 to F5, are available to cover the far range of the swath with incidence angle ranges from 37° to 47°. By modifying timing parameters, 10 new positions have been added with offset ground coverage. Each original Fine beam position can either be shifted closer to or farther away from Nadir. The resulting positions are denoted by either an N (Near) or F (Far). For example, F1 is now complemented by F1N and F1F (RADARSAT 2011). Finally, RADARSAT-1 requires 24 days to return to its original orbit path. This means that for most geographic regions, it will take 24 days to acquire exactly the same image (the same beam mode, position, and geographic coverage). However, RADARSAT's imaging flexibility allows images to be acquired on a more frequent basis (RADARSAT 2011).

3.2 Ground data

Following Marghany et al., (2010b), the GPS survey used to: (i) to record exact geographical position of shoreline; (ii) to determine the cross-sections of shore slopes; (iii) to corroborate the reliability of DInSAR data co-registered; and finally, (iv) to create a reference network for future surveys. The geometric location of the GPS survey was obtained by using the new

satellite geodetic network, IGM95. After a careful analysis of the places and to identify the reference vertexes, we thickened the network around such vertexes to perform the measurements for the cross sections (transact perpendicular to the coastline). The GPS data collected within 20 sample points scattered along 400 m coastline. The interval distance of 20 m between sample location is considered. In every sample location, Rec-Alta (Recording Electronic Tacheometer) was used to acquire the spit elevation profile. The ground truth data were acquired on 23 December 2003 March 26, 2005, during satellite passes. Then ground data used to validate and find out the level of accuracy for DInSAR and fuzzy B-spline algorithm.

4. DInSAR data processing

The DInSAR technique measures the block displacement of land surface caused by subsidence, earthquake, glacier movement, and volcano inflation to cm or even mm accuracy (Luo et al., 2006). According to Lee (2001), the surface displacement can estimate using the acquisition times of two SAR images S_1 and S_2. The component of surface displacement thus, in the radar-look direction, contributes to further interferometric phase (φ) as

$$\phi = \frac{4\pi}{\lambda}(\Delta R + \zeta) \tag{1}$$

where ΔR is the slant range difference from satellite to target respectively at different time, λ is the RADARSAT-1 SAR fine mode wavelength which is about 5.6 cm for CHH- band. According to Lee (2001), for the surface displacement measurement, the zero-baseline InSAR configuration is the ideal as $\Delta R = 0$, so that

$$\phi = \phi_d = \frac{4\pi}{\lambda}\zeta \tag{2}$$

In practice, zero-baseline, repeat-pass InSAR configuration is hardly achievable for either spaceborne or airborne SAR. Therefore, a method to remove the topographic phase as well as the system geometric phase in a non-zero baseline interferogram is needed. If the interferometric phase from the InSAR geometry and topography can strip of from the interferogram, the remnant phase would be the phase from block surface movement, providing the surface maintains high coherence (Luo et al., 2006).

Zebker et al. (1994) and Luo et al., (2006) used the three-pass method to remove topographic phase from the interferogram. This method requires a reference interferogram, which is promised to contain the topographic phase only. The three-pass approach has the advantage in that all data is kept within the SAR data geometry while DEM method can produce errors by misregistration between SAR data and cartographic DEM. The three-pass approach is restricted by the data availability. The three-passes DInSAR technique uses another InSAR pair as a reference interferogram that does not contain any surface movement event as

$$\phi' = \frac{4\pi}{\lambda}\Delta R' \cdot \tag{3}$$

Incorporating equations 2 and 3 gives the phase difference, only from the surface displacement as

$$\phi_d = \phi - \frac{\Delta R}{\Delta R'}\phi' = \frac{4\pi}{\lambda}\zeta \cdot \tag{4}$$

For an exceptional case where $\frac{\Delta R}{\Delta R'}$ in equation 4 there is a positive integer number, phase unwrapping may not be necessary (Massonnet et al., 1998). However, this is not practical and it is difficult to achieve from the system design for a repeat-pass interferometer. From equation 4 the displacement sensitivity of DInSAR is given as

$$\frac{\partial \phi_d}{\partial \zeta} = \frac{4\pi}{\lambda}. \tag{5}$$

Marghany and Mazlan (2009) introduces a method to construct 3-D object visualisation from unwrapping phase as follow,

$$S(p,q) = \frac{\sum_{i=0}^{M}\sum_{j=0}^{O}\phi_d C_{ij}\beta_{i,4}(p)\beta_{j,4}(q)w_{i,j}}{\sum_{m=0}^{M}\sum_{l=0}^{O}\beta_{m,4}(p)\beta_{l,4}(q)w_{ml}} = \sum_{i=0}^{M}\sum_{j=0}^{O}\phi_d C_{ij}S_{ij}(p,q) \tag{6}$$

where $\beta_{i,4}(p)$ and $\beta_{j,4}(q)$ are two bases of B-spline functions, $\{C_{ij}\}$ is the bidirectionally control net and $\{w_{ij}\}$ is the weighted correlation coefficient which was estimated based on Marghany (2011) as

$$w_{ij} = \frac{\left| \frac{\sum S_M(i,j)S_s(i,j)}{\sqrt{\sum |S_M(i,j)|^2 \sum |S_s(i,j)|^2}} \right| x \min(|S_M(i,j)|, |S_s(i,j)|) - t_1}{t_2 - t_1} \tag{7}$$

where $|S_M(i,j)|$ and $S_s(i,j)$ are master and slave complex data while t_1 and t_2 are thresholds. The curve points *S(p,q)* are affected by $\{w_{ij}\}$ in case of $p \in [r_i, r_{i+P+1}]$ and $q \in [r_j, r_{j+P'+1}]$, where *P* and *P′* are the degree of the two B-spline basis functions constituted the B-spline surface. Two sets of knot vectors are knot *p*=[0,0,0,0,1,2,3,……,*O*,*O*,*O*,*O*], and *knot q*=[0,0,0,0,1,2,3,….,*M*,*M*,*M*,*M*]. Fourth the order B-spline basis are used $\beta_{j,4}(.)$ to ensure the continuity of the tangents and curvatures on the whole surface topology including at the patches' boundaries (Marghany 2011).

5. Three-dimensional SPIT visualization using DInSAR technique

The new fuzzy B-spline formula for 3D coastal features' reconstruction from DInSAR retrieved unwrapping phase was trained on three RADARSAT-1 SAR fine mode data (Fig.2). The master data was acquired on 23 November 1999, the slave 1 data was acquired on 23 December 2003, while slave 2 data acquisition was on 26 March 2005, respectively. The

master data was ascending while both slave data were descending. Figure 2 shows the variation of the backscatter intensity for the F1 mode data along Terengganu's estuary. The urban areas have the highest backscatter of-10 dB as compared to water body and the vegetation area (Fig. 2).

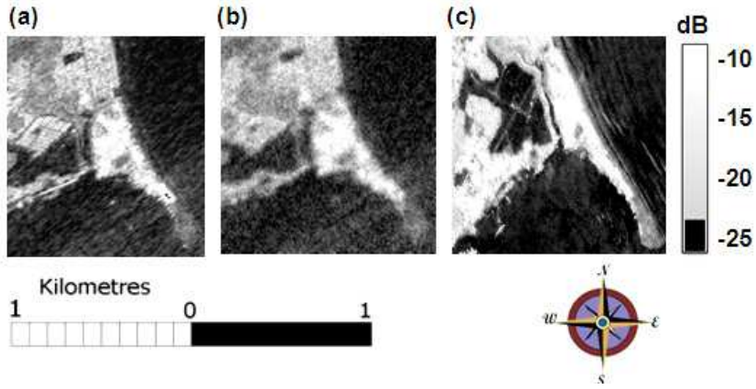

Fig. 2. RADARSAT-1 SAR fine mode data acquisition (a) master data, (b) data slave 1 data and (c) slave 2 data.

It is interesting to find the coherence image coincided with backscatter variation along the coastal zone. Fig. 3(a) shows that urban zone dominated with higher coherence of 0.8 than vegetation and sand areas. The coastal spit has lower backscatter and coherence of 0.3 dB and 0.25, respectively. Since three F1 mode data acquired in wet north-east monsoon period, there is an impact of wet sand on radar signal penetration which causing weak penetration of radar signal because of dielectric. Figure 3b shows the ratio coherence image, clearly the total topographic decorrelation effects along the radar-facing slopes are dominant and highlighted as bright features of 3 over a grey background. This is caused by the micro-scale movement of the sand particles driven by the coastal hydrodynamic, and wind continuously changes the distribution of scatterers resulting in rapid temporal decorrelation which has contributed to decorrelation in the spit zone.

Clearly, the random changes in the surface scatterer locations among data acquisitions with a wavelength of 5.6 cm for C-band are sufficient to decorrelate the interferometric signal. Under this circumstance, it will be visible in the coherence data (Fig.3). Since vegetation and wet sand changes may also reduce the coherence because the estuary area has tides and water lines that are so highly variable, this can be defined in fuzzy or probabilistic terms. The geomorphology feature of spit is rendered meaningless or unreliable in the long term because of their high variability. This confirms the studies of of Hanssen (2001); Marghany and Hashim (2009); and Rao and Jassar (2010); Marghany (2011).

Further, the estimated baseline is varied between master data and both slave data. The estimated baseline between master data and second slave data is 400 m which is larger than slave 1 data (Table 1). In this context, Gens (2000) reported the length of the baseline designates the sensitivity to height changes and sum of baseline decorrelation. Further, Nizalapur et al., (2011) stated the time difference for two data acquisitions is a second source of decorrelation. Indeed, the time difference while comparing data sets with a similar baseline length acquired one and 35 days a part suggest only the temporal component of

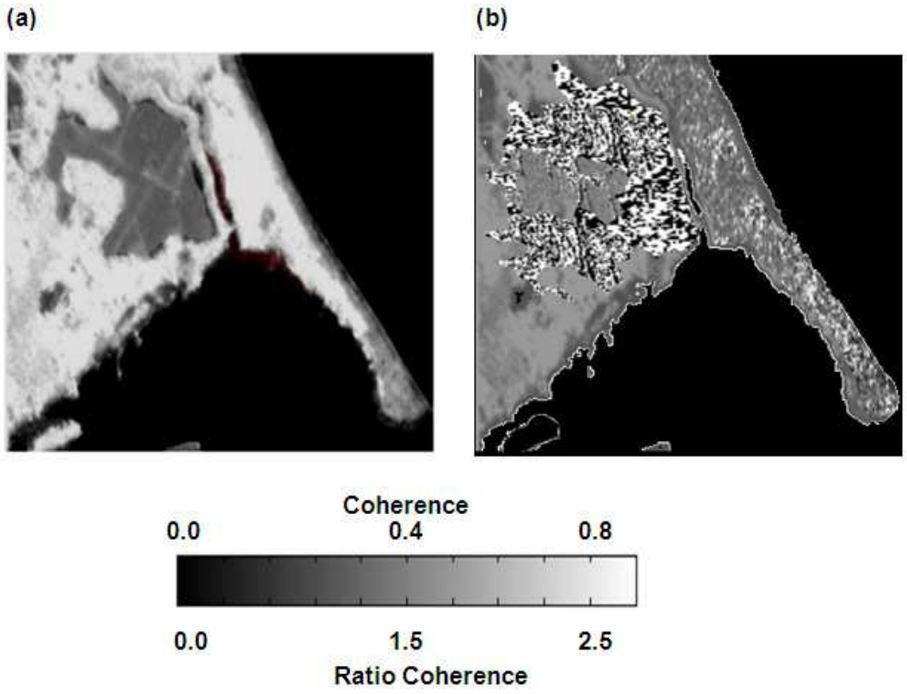

Fig. 3. Variation of (a) coherence and (b) ratio coherence in F1 mode data.

the decorrelation. Therefore, the loss of coherence in the same repeat cycle in data acquisition are most likely because of baseline decorrelation.

Acquisition Data	Baseline	Wind Speed (m/s)	Tidal (m)
23 November 1999	345	7.3	1.2
23 December 2003	266	9	1.5
26 March 2005	400	11	1.8

Table 1. Baseline estimations with wind and tidal conditions during acquisition time.

Evidently, wind speed of 11 m/s affects the scattering from certain vegetation classes and sandy regions and consequently produce poor coherence (Table 1). The overall scene is highly incoherent, not only because of the meteorological conditions and the vegetation cover at the time but also because of ocean surface turbulent changes. This decorelation caused poor detection of spit which induce large ambiguities because of poor coherence and scattering phenomenology. The ground ambiguity and ideal assumption that volume-only coherence can be acquired in at least one polarization. This assumption may fail when vegetation is thick, dense, or the penetration of electromagnetic wave is weak. This is agreed with study of Lee (2001).

Fig. 4 shows the interferogram created from F1 data. For three data sets, only small portion of the scene processed because of temporal decorrelation. According to Luo et al.,(2007), the SAR interferogram is considered to be difficult to unwrap because of its large areas of low

coherence, which caused by temporal decorrelation. These areas of low coherence segment the interferogram into many pieces, which creates difficulties for the unwrapping algorithms (Fig.4). In this context, Lee (2001) reported that when creating an interferogram of surface deformation by using InSAR, it is not always true that an interference pattern (fringes) of an initial interferogram directly shows surface deformation. Indeed, the difference in phase between two observations is influenced by things outside surface deformation.

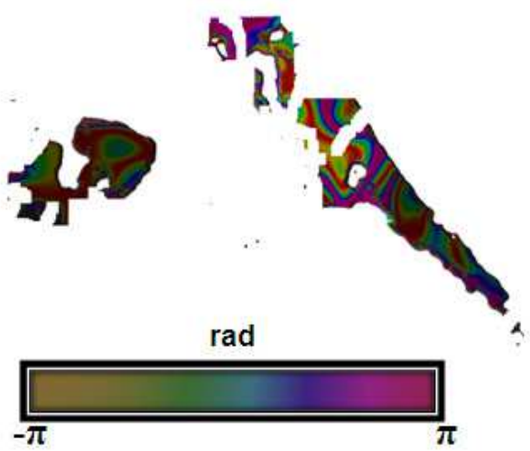

Fig. 4. Interfeorgram generated from F1 mode data.

Figure 5 shows the interferogram created using fuzzy B-spline algorithm. The full color cycle represents a phase cycle, covering range between –π to π. In this context, the phase difference given module 2 π; is color encoded in the fringes. Seemingly, the color bands change in the reverse order, indicating that the center has a great deformation along the spit. This shift corresponds to 0.4 centimetres (cm) of coastal deformation over the distance of 500 m. The urban area dominated by deformation of 2.8 cm.

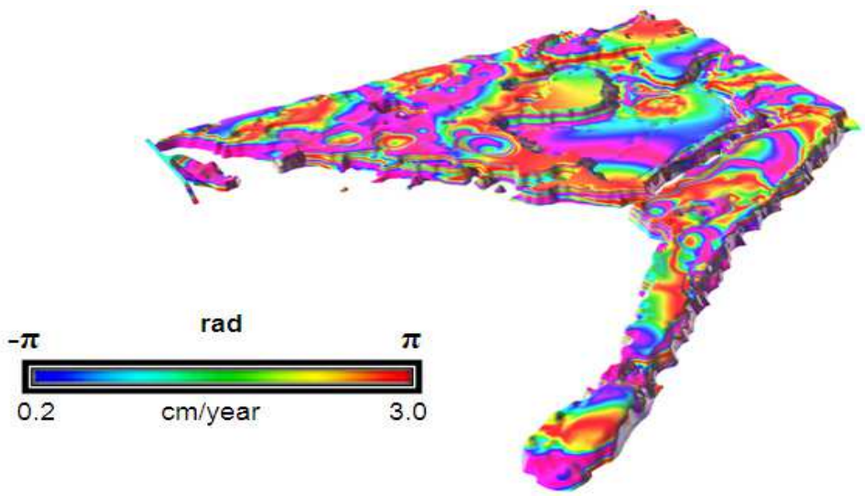

Fig. 5. Fringe Interferometry generated by fuzzy B-spline.

Fig. 6 represents 3-D spit reconstruction using fuzzy B-spline with the maximum spit 's elevation is 3 m with gentle slope of 0.86 m. The rate change of spit is 3 m/year with maximum elevation height of 2.4 m (Figs 5 and 6). Clearly, Terengganu 's spit was generated due to the deposition of sediment due to hydrodynamic changes between estuary and ocean. According to Marghany (2012) Terengganu 's mouth river is the largest hydrologic communication between an estuary and the South China Sea. This spit occurred when longshore drift reaches a section of Terengganu's River where the turn is greater than 30 degrees. It continued out therefore, into the sea until water pressure from a Terengganu 's River becomes too much to allow the sand to deposit. The spit be then grown upon and become stable and often fertile. As spit grows, the water behind them is sheltered from wind and waves. This could be due the high sediment transport through the water outflow from the river mouth, or northerly net sediment transport due to northeast monsoon wave effects (Marghany et al., 2010b). Longshore drift (also called littoral drift) occurs due to waves meeting the beach at an oblique angle, and back washing perpendicular to the shore, moving sediment down the beach in a zigzag pattern. Longshore drifting is complemented by longshore currents, which transport sediment through the water alongside the beach. These currents are set in motion by the same oblique angle of entering waves that cause littoral drift and transport sediment in a similar process. The hydrodynamic interaction between the longshore current and water inflow from the Terengganu Mouth River is causing the changes in spit's geomorphology characteristics. This finding confirms the study of Marghany et al., (2010a) ; Marghany et al., (2010b) and Marghany (2011). The increasing growth of spit across the estuary is due to impact of sedimentation due to littoral drift. According to Marghany and Mazlan (2010a) net littoral drift along Kuala Terengganu coastal water is towards the southward which could induce the growth of spit length.

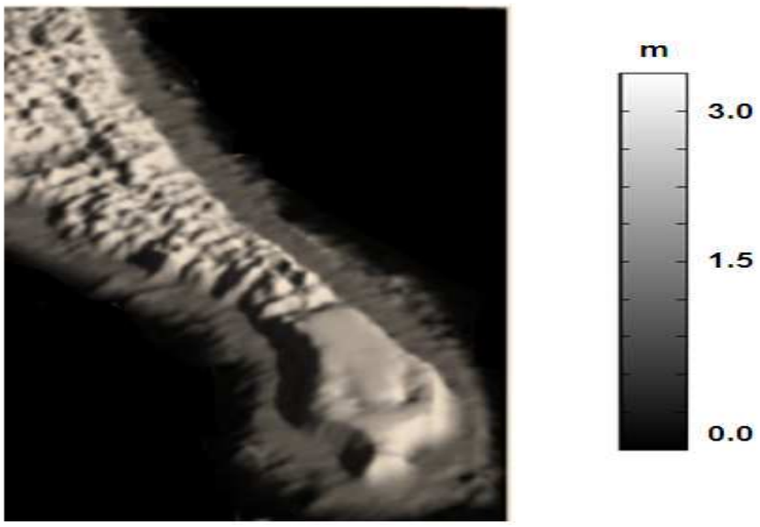

Fig. 6. DEM of coastal spit.

Finally, a difference statistical comparison confirms the results of Figs 4,5 and 6. Table 2 shows the statistical comparison between the simulated DEM from the DInSAR, real ground measurements and with using fuzzy B-spline. This table represents the bias (averages mean the standard error, 90 and 95% confidence intervals, respectively. Evidently, the DInSAR

using fuzzy B-spline performance has bias of-0.05 m, lower than ground measurements and the DInSAR method. Therefore, fuzzy B-spline has a standard error of mean of ± 0.034 m, lower than ground measurements and the DInSAR method. Overall performances of DInSAR method using fuzzy B-spline is better than DInSAR technique which is validated by a lower range of error (0.02±0.21 m) with 90% confidence intervals.

Statistical Parameters	**DInSAR techniques**			
	DInSAR		**DInSAR-Fuzzy B-spline**	
Bias	2.5		-0.05	
Standard error of the mean	1.5		0.034	
	Lower	**Upper**	**Lower**	**Upper**
90 % (90 % confidence interval)	1.2	2.6	0.02	0.16
95 % (95 % confidence interval)	0.98	2.35	0.03	0.21

Table 2. Statistical Comparison between DInSAR and DInSAR-Fuzzy B-spline Techniques.

Fuzzy B-spline produced perfect pattern of fringe interfeormetry compared with one produced by DInSAR technique (Fig. 5). It shows there are many deformations of over several centimetres. In these deformations, it is known the deformation in spit because of coastline sedimentation. The other deformations, however, are caused not by the movement of the coastal sediment but the spatial fluctuation of water vapour in the atmosphere. In addition, the growths of urban area induces also land cover changes. Further, it can be noticed that fuzzy B-spline preserves detailed edges with discernible fringes (Russo 1998 and Rövid et al. 2004). Indeed, Fig 5. shows smooth interferogram, in terms of spatial resolution maintenance, and noise reduction, compared to conventional methods (Zebker et al.,1997; Massonnet, and Feigl 1998; Burgmann et al., 2000; Hanssen 2001; Yang et al., 2007; Rao and Jassar (2010).

This has been contributed since each operation on a fuzzy number becomes a sequence of corresponding operations on the respective μ -levels , and the multiple occurrences of the same fuzzy parameters evaluated because of the function on fuzzy variables (Anile et L., 1995 and Anile et al., 2000). It is easy to distinguish between small and long fringes. Typically, in computer graphics, two objective quality definitions for fuzzy B-spline were used: triangle-based criteria and edge-based criteria. Triangle-based criteria follow the rule of maximization or minimization, respectively, of the angles of each triangle (Fuchs et al. 1997). The so-called max-min angle criterion prefers short triangles with obtuse angles. This result agrees confirms the studies of Anile et al. (2000); Marghany et al.,(2010a); and Marghany (2011).

6. Conclusions

Synthetic Aperture Radar interferometry (InSAR) is a relatively new technique for 3-D topography mapping. This study presents a new approach for 3-D object simulation using Differential synthetic aperture interferometry (DInSAR). This work has demonstrated the 3-D spit reconstruction from DInSAR using three C-band SAR images acquired by RADARSAT-1 SAR F 1 mode data. The conventional method of DInSAR used to create 3-D coastal geomorphology reconstruction. Nevertheless, it was difficult to generate phase and

interfeorgram using conventional DInSAR because of temporal decorrelation. The result shows that spit and vegetation zone have poor coherence of 0.25 as compared to the urban area. In addition, only small portion of the F1 mode scene was processed because of temporal decorrelation. Finally, the fuzzy B-spline algorithm used to reconstruct fringe pattern, and 3-D from decorrelate unwrap phase. The fringe pattern shows the deformation of 0.4 cm along spit and 1.4 cm in urban area. Further, the maximum 3-D spit elevation is 3 m with the standard error of mean of ± 0.034 m. In conclusion, the integration between the conventional DInSAR method and the FBSs could be an excellent tool for 3-D coastal geomorphology reconstruction from SAR data the under circumstance of temporal decorrelation.

7. References

Anile, A.M., B. Falcidieno, G. Gallo, M. Spagnuolo, S. Spinello, (2000). "Modeling uncertain data with fuzzy B-splines", Fuzzy Sets and Syst. 113, 397-410.

Anile, AM, Deodato, S, Privitera, G, (1995) *Implementing fuzzy arithmetic*, Fuzzy Sets and Systems, 72,123-156.

Askne, J., M. Santoro, G. Smith, and J. E. S. Fransson (2003). "Multitemporal repeat-pass SAR interferometry of boreal forests," *IEEE Trans. Geosci. Remote Sens.* 41, 1540–1550.

Burgmann, R., P.A. Rosen, and E.J. Fielding (2000). "Synthetic aperture radar interferometry to measure Earth's surface topography and its deformation", *Ann. Rev.of Earth and Plan. Sci.* 28: 169–209.

Fuchs, H. Z.M. Kedem, and Uselton, S.P., (1977). Optimal Surface Reconstruction from Planar Contours. *Communications of the ACM*, 20, 693-702.

Gens,R., (2000)."The influence of input parameters on SAR interferometric processing and its implication on the calibration of SAR interferometric data", *Int. J. Remote Sens.* 2,11767–1771.

Hanssen R.F., (2001). *Radar Interferometry: Data Interpretation and Error Analysis*, Kluwer Academic, Dordrecht, Boston.

Lee H., (2001). "Interferometric Synthetic Aperture Radar Coherence Imagery for Land Surface Change Detection" Ph.D theses, University of London.

Luo, X., F.Huang, and G. Liu, (2006). "Extraction co-seismic Deformation of Bam earthquake with Differential SAR Interferometry". *J. New Zea. Inst. of Surv*. 296:20-23.

Massonnet, D. and K. L. Feigl (1998).,"Radar interferometry and its application to changes in the earth's surface,"*Rev. Geophys.* 36, 441–500 .

Marghany M (2012). 3-D Coastal Bathymetry Simulation from Airborne TOPSAR Polarized Data. "*Bathymetry and Its Applications*". In Ed., Blondel P., InTech - Open Access Publisher, University Campus STeP Ri, Croatia, 57-76.

Marghany M (2011).Three-dimensional visualisation of coastal geomorphology using fuzzy B-spline of dinsar technique. Int. J. of the Phys. Sci. 6(30):6967 – 6971.

Marghany,M., M. Hashim and A. P. Cracknell, (2010a)."3-D visualizations of coastal bathymetry by utilization of airborne TOPSAR polarized data". *Int. J. of Dig. Earth*, 3,187 – 206.

Marghany, M., and M. Hashim (2009).“Differential Synthetic Aperture radar Interferometry (DInSAR) for 3D Coastal Geomorphology Reconstruction”. IJCSNS Int. J. of Comp. Sci. and Network Secu., 9,59-63.

Marghany, M., and M. Hashim (2010a).“Different polarised topographic synthetic aperture radar (TOPSAR) bands for shoreline change mapping. *Int. J. Phys. Sci. 5*, 1883-1889.

Marghany, M.,Z. Sabu and M. Hashim,(2010b) “Mapping coastal geomorphology changes using synthetic aperture radar data”. *Int. J. Phys. Sci. 5,*1890-1896.

Marghany M., and M. Hashim (2010b). “Velocity bunching and Canny algorithms for modelling shoreline change rate from synthetic aperture radar (SAR). *Int. J. Phys. Sci. 5,*1908-1914.

Nizalapur, V., R. Madugundu, and C. Shekhar Jha (2011). “Coherence-based land cover classification in forested areas of Chattisgarh, Central India, using environmental satellite—advanced synthetic aperture radar data”, *J. Appl.Remote Sens.* 5, 059501-1-059501-6.

RADARSAT International, (2011)“RADARSAT application [online] Available from http:\www.rsi.ca [Accessed 8 June 2011].

Rao, K.S., H. K. Al Jassar, S. Phalke, Y. S. Rao, J. P. Muller, and. Z. Li, (2006). "A study on the applicability of repeat pass SAR interferometry for generating DEMs over several Indian test sites," *Int. J. Remote Sens.* 27, 595–616.

Rao, K.S.,and H. K. Al Jassar (2010). “Error analysis in the digital elevation model of Kuwait desert derived from repeat pass synthetic aperture radar interferometry”, *J. Appl.Remote Sens*.4,1-24.

Russo, F., (1998).Recent advances in fuzzy techniques for image enhancement. IEEE Transactions on Instrumentation and measurement. 47, pp: 1428-1434.

Rövid, A., Várkonyi, A.R. andVárlaki, P., (2004). 3D Model estimation from multiple images,” IEEE International Conference on Fuzzy Systems, FUZZ-IEEE’2004, July 25-29, 2004, Budapest, Hungary, pp. 1661-1666.

Yang, J., T.Xiong, and Y. Peng, (2007). “A fuzzy Approach to Filtering Interferometric SAR Data”. *Int. J. of Remote Sens*., 28, 1375-1382.

Zebker, H.A., C.L.,Werner, P.A. Rosen, and S. Hensley, (1994). "Accuracy of Topographic Maps Derived from ERS-1 Interferometric Radar", *IEEE Geosci. Remote Sens.*,2,823-836.

Zebker, H.A., P.A. Rosen, and S. Hensley (1997)."Atmospheric effects in inteferometric synthetic aperture radar surface deformation and topographic maps", *J. Geophys. Res.*102, 7547–7563.

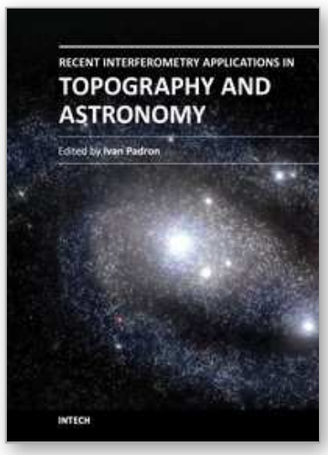

Recent Interferometry Applications in Topography and Astronomy
Edited by Dr Ivan Padron

ISBN 978-953-51-0404-9
Hard cover, 220 pages
Publisher InTech
Published online 21, March, 2012
Published in print edition March, 2012

This book provides a current overview of the theoretical and experimental aspects of some interferometry techniques applied to Topography and Astronomy. The first two chapters comprise interferometry techniques used for precise measurement of surface topography in engineering applications; while chapters three through eight are dedicated to interferometry applications related to Earth's topography. The last chapter is an application of interferometry in Astronomy, directed specifically to detection of planets outside our solar system. Each chapter offers an opportunity to expand the knowledge about interferometry techniques and encourage researchers in development of new interferometry applications.

INTECH
open science | open minds

InTech Europe
University Campus STeP Ri
Slavka Krautzeka 83/A
51000 Rijeka, Croatia
Phone: +385 (51) 770 447
Fax: +385 (51) 686 166
www.intechopen.com

InTech China
Unit 405, Office Block, Hotel Equatorial Shanghai
No.65, Yan An Road (West), Shanghai, 200040, China
中国上海市延安西路65号上海国际贵都大饭店办公楼405单元
Phone: +86-21-62489820
Fax: +86-21-62489821

IntechOpen